Heat Transfer in Reciprocating Compressors - Compressor3D

H. Steinück[*], T. Müllner

September 5, 2022

Contents

---

[*]Vienna University of Technology, Institute of Fluid Mechanics and Heat Transfer, Getreidemarkt 9, 1060 Vienna, Austria E-mail: herbert.steinrueck@tuwien.ac.at, Phone +43 1 58801 32231

List of Figures

List of Tables

1 Introduction

Based on the success of Compressor1D and Compressor2D for the description of internal waves and their interaction with the valves, it was suggested to extend these programs to a heat transfer analysis of the compressor, see [1], [3], [2].

Identifying dimensionless numbers (Stanton numbers), which relate the mass flow and piston velocity to heat transfer coefficients, a new version of compressor1D has been released, which gives an educated guess of the heat transfer coefficients from the gas to the cylinder wall, head, and piston. However, these Stanton numbers had been the result of numerous CFD simulation using a commercial CFD Program (FLUENT) to simulate the flow and heat transfer in a reciprocating compressor.

Due to the complex flow field in a compressor, a 3-dimensional description of the flow field for the heat transfer is necessary. The first idea was to use a combination of a 1D-flow field in the valve pockets and a three 3D simulation in the interior of the cylinder. A similar approach had been successfully used in Compressor2D. However, the interface conditions between the 1D flow region and the interior of the cylinder turned out to be more difficult than it was in the 2D case. Thus, a complete 3D flow simulation of the flow in the compressor has been realized.

Part of the concept was to simulate the inviscid Euler flow only and calculate the heat transfer a posteriori by a boundary-layer calculation.

In section 2 we will summarize and discuss the model assumptions, in section 3 we will describe the numerical methods, section 4 is devoted to the program description as a users guide, and in section 5 we will discuss two example solutions.

2 Physical models

2.1 Flow model

If we estimate the Reynolds number of the gas flow in the compressor with typical piston velocities and typical cylinder diameters, we obtain for the Reynolds number of the gas flow values larger than 50000. Thus, we expect that the flow is on one hand turbulent on the other hand almost inviscid. However, the flow velocities may change during a compression cycle drastically. Usually, the design of a compressor is such that supersonic flow is avoided. However, the flow may be transonic locally during intake and discharge. Thus, the governing equation will be the continuity equation

$$\frac{\partial}{\partial t}\rho + \frac{\partial}{\partial x}\rho u + \frac{\partial}{\partial x}\rho v + \frac{\partial}{\partial x}\rho w = 0, \tag{1}$$

the momentum equations written in conservative form

$$\frac{\partial}{\partial t}\begin{pmatrix} \rho u \\ \rho v \\ \rho w \end{pmatrix} + \frac{\partial}{\partial x}\begin{pmatrix} \rho u^2 + p \\ \rho uv \\ \rho uw \end{pmatrix} + \frac{\partial}{\partial y}\begin{pmatrix} \rho uv \\ \rho v^2 + p \\ \rho vw \end{pmatrix} + \frac{\partial}{\partial z}\begin{pmatrix} \rho uw \\ \rho wv \\ \rho w^2 + p \end{pmatrix} = 0, \tag{2}$$

where u, v, w denote velocity components in the x, y, z-direction, respectively, of a Cartesian coordinate system, and the energy equation

$$\frac{\partial}{\partial t}e_{tot} + \frac{\partial}{\partial x}\left[\rho u\left(e_{tot} + \frac{p}{\rho}\right)\right] + \frac{\partial}{\partial y}\left[\rho v\left(e_{tot} + \frac{p}{\rho}\right)\right] + \frac{\partial}{\partial z}\left[\rho w\left(e_{tot} + \frac{p}{\rho}\right)\right] = 0, \tag{3}$$

where the specific total energy

$$e_{tot} = e_{\mathrm{n}} + \frac{u^2 + v^2 + w^2}{2} \tag{4}$$

is the sum of the specific internal energy e_{in} and the kinetic energy. Additionally, equations of state, which relate the thermodynamic quantities, have to be specified. The Program Compressor 3D is restricted to

ideal gases with constant specific heat capacities.

$$\frac{p}{\rho} = (c_p - c_v)T, \qquad e_{\text{in}} = c_v T, \tag{5}$$

where c_v. c_p are the specific iso-choric and iso-baric specific heat capacities, respectively. The absolute temperature is denoted by T.

2.2   Valve model

2.2.1   Valve Dynamic

The discharge and the suction valves are located adjacent to the circular lateral surfaces of the valve pockets. Both valves are unidirectional restrictor valves, plate valves or ring valves are usually used. In this work we concentrate on plate valves but most of the equations can be easily adopted to any kind of restrictor valve. Figure 1 shows the basic function of a plate valve, see [1]. The state of a valve is
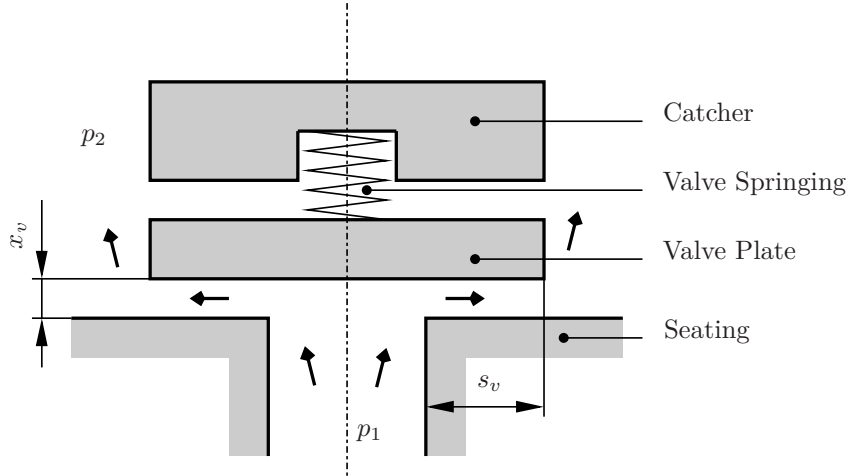
Figure 1: Schema of a plate valve.

specified by the distance between the valve plate and the seating x_v. The motion of the valve plate is determined by the forces acting on it. We consider the following three contributions to the resulting force: the pressure difference across the valve acting on an effective force area A_F of the valve plate, the springing and thirdly a contribution due to viscous forces in the initial stages of valve opening. Denoting the average pressure in front of the valve $\bar{p}_1$ and behind the valve $\bar{p}_2$, we obtain the equation of motion for the valve plate

$$m_v \ddot{x}_v = (\bar{p}_1 - \bar{p}_2)A_F , \tag{6}$$

Here, m_v stands for the mass of the valve plate. The constants c_s and l_1 denote spring constant and initial deflection of the spring, respectively.

The motion of the valve plate is limited by the seating on one side and by the catcher on the other side. Therefore the deflection of the plate x_v ranges from $x_{v,min}$ to $x_{v,max}$. Due to the fact that the flow within the valve changes with x_v, and thus the effective force area A_v changes, we introduce a force coefficient c_F. The force area A_F can be written as

$$A_F = A_{F,0}c_F , \tag{7}$$

where $A_{F,0}$ stands for the force area at closed valve. For common plate valves the relation between the force coefficient and valve lift takes the form

$$c_F = \left(1 - 0.2\frac{x_v}{x_{v,max}}\right). \tag{8}$$

2.2.2 Flow through the valve

The flow through the valves is considered as (quasi stationary) outflow of gas from a pressurized vessel through a convergent nozzle. In case of constant heat capacities the mass flow density j is given by St.Venant and Wantzell [5]

$$j = \dot{m} = \frac{1}{A_V} \phi \rho_1 \left(\frac{p_2}{p_{t1}}\right)^{\frac{1}{\gamma}} \sqrt{\frac{2\gamma}{\gamma-1} \frac{p_{t1}}{\rho_1} \left(1 - \left(\frac{p_2}{p_{t1}}\right)^{\frac{\gamma-1}{\gamma}}\right)} , \qquad (9)$$

where A_V is the valve cross section and p_{t1} are the total pressures before and p_2 is the pressures after the valve, respectively. Note, p_2 and p_t may vary along the valve.

The effective flow cross section ϕ of the valve is assumed to be a function of the position of the valve plate x_v only. This is not true if effects of asymmetric flow conditions in the valve pocket are taken into account. For common valves the equation for the effective cross section takes the form

$$\phi(x_v) = \sqrt{\frac{(f_{e1mm} x_v)^2}{\alpha_v + \beta_v x_v{}^2}} . \qquad (10)$$

The constant f_{e1mm} denotes the valve flow cross-section when the valve plate is 1 mm above the valve seating. The constants α_v and β_v describe non-linear dependencies of the valve plate lift and have to be determined empirically.

2.3 Heat transfer model

The heat transfer coefficients will be calculated as a post processing of the inviscid Euler-flow simulation. Thus, we have implicitly assumed that the heat transfer from outside to the core region of the flow does not influence the flow field, the pressure, and density distribution. For the heat transfer analysis we assume that the internal (inviscid) flow field is given and the heat transfer to the cylinder wall, piston and cylinder head will be determined by a posteriori boundary-layer calculation.

Thus, we assume that the characteristic Reynolds $\mathrm{Re} = U_p d/\nu$ number is sufficiently large. In that case, the flow field flow field can be decomposed into an inviscid flow region and a boundary-layer flow, which consists of the defect-layer and the viscous sub-layer, [4] p.517. The structure of the flow field in these layers is given by

- defect layer: $u = U_{in} - u_\tau f'(y^+ Re_\tau)$

- overlap region: $u = u_\tau \left(\frac{1}{\kappa} \ln y^+ + C_2\right)$

- viscous sub-layer $u = u_\tau f(y^+)$

where the friction velocity u_τ and the and the dimensionless wall coordinate y^+ are defined by:

$$u_\tau^2 = \frac{\tau_w}{\rho}, \quad y_+ = \frac{y u_\tau}{\nu}, \quad Re_\tau = \frac{u_\tau \delta}{\nu}.$$

Here, δ denotes the boundary layer thickness.

Assuming a high Reynolds-number attached boundary-layer flow, the velocity profile of the defect-layer and the viscous sub-layer must overlap and in the overlap region and must be asymptotically equal. This, yields the friction law:

- friction law:

$$\frac{U}{u_\tau} = \frac{1}{\kappa} \ln \frac{u_\tau \delta}{\nu} + C^+ + \frac{2\Pi(x)}{\kappa} \approx \frac{1}{\kappa} \ln \frac{u_\tau \delta}{\nu} + C^+ \quad , \quad \kappa = 0.40 \quad \text{von Karman const.}$$

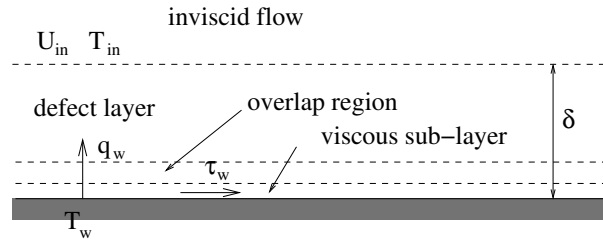- friction velocity $u_\tau = \sqrt{\frac{\tau_w}{\rho}}$,

Figure 2: Structure of an attached turbulent boundary-layer

- friction coefficient: $\quad c_f = \dfrac{2\tau_w}{\rho U^2} = 2\dfrac{u_\tau^2}{U^2}$.

The constant C^+ depends on the velocity profile in the viscous sub-layer and is a function of the wall roughness only. $\Pi(x)$ depends on the velocity profile in the defect layer and δ is the yet unknown boundary layer thickness.

In order to determine the missing quantities one has to solve the boundary-layer equation in the defect region. The following three strategies can be followed:

a) Solve the boundary-layer equations (finite volume method). A turbulence model has to be chosen.

b) Solve boundary-layer equations with an integral method for δ. A suitable velocity profile has to be chosen.

c) Estimate boundary layer thickness for each face.

For simplicity we have chosen strategy c) assuming the simplest boundary-layer structure see [4] p. 581.

$$c_f = 2 \left(\frac{\kappa}{\ln \mathrm{Re}} \underbrace{G(\Lambda, D)}_{\sim 1.5} \right)^2 \tag{11}$$

Using the Reynolds analogy for the heat transfer, we obtain for the heat transfer coefficient, see [4] (18.157]

$$\alpha_{ave} = \rho c_p U_{ave} \mathrm{St}, \quad \mathrm{St} = \frac{1}{\mathrm{Pr}_t} \frac{c_f}{2},$$

where St is the Stanton number which relates the wall heat flux density $\dot{q}$ to an appropriate enthalpy flux density $\rho u c_p \Delta T$ based on the inviscid flow velocity along the wall. The turbulent Prandtl number is assumed to be constant, $\mathrm{Pr}_t = 0.87$. The velocity u_{ave} is the momentary mean velocity of the inviscid flow field over the the face (piston, head, side wall) under consideration.

The heat transfer coefficients are stored in the file alpha_on_HSP.txt.

2.3.1   Release note 23.4.2015

The current version of Compressor3D calculates the average heat transfer coefficients for each face (piston, head and side wall) as a function of the crank angle. At the moment the material properties of the gas are hard coded for air. In a later version an option to choose the material properties will be included.

3   Numerical issues

3.1   Geometry and mesh

The domain of the flow simulation consists of the interior of the compressor between the cylinder head and the movable piston and a (variable) number of valve pockets which connect the the cylinder with the valves.

3.1.1 Cylinder

Due to the simple geometry of the cylinder inside the cylinder a layered structured mesh is used. The grid lines in the plane of the cylinder head are shown in figure 5 for a compressor with 5 suction and 5 discharge valves. In this example there are $n_R = 15$ cells along the radius of the cylinder. In the vertical direction (along the cylinder axis) the cell size depends on the piston of the cylinder. The cells are evenly distributed in vertical direction. If the the aspect ratio of the cells are below or above certain thresholds, a new mesh will be generated and the cell averages of the computational quantities will be redistributed to the new cells in a conservative manner. The minimum number of cells in $z-$direction is 2, when the piston in the position of minimal volume.

3.1.2 Valve Pockets

The valve pockets are meshed with an unstructured tetrahedra mesh. For a compressor simulation one prototype of a valve mesh has to be generated. One prototype valve mesh will be delivered with Compressor3D in the file `reference_valve_pocket.msh`. This reference mesh will scaled to fit the actual dimensions. Moreover, copies of this mesh will be used for all valve pockets. Thus, for each valve pocket the position, angle φ, see figure 5, has to be specified. The prototype file has to have the format shown in table 1.:

line number	col 1	col 2	col 3	col 4	col 5	col 6	col 7	col 8	comment
1	N_P								number of vertices
2	x_1	y_1	z_1						coordinates of vertices
.	..	..	..	..	..	..	..	..	
$N_p + 1$	x_{N_p}	y_{N_p}	z_{N_p}						
$N_p + 2$	N_T								number of tetrahedra
$N_p + 3$	$p_{1,1}$	$p_{2,1}$	$p_{3,1}$	$p_{4,1}$	$f_{1,1}$	$f_{2,1}$	$f_{3,1}$	$f_{4,1}$	indices of the 4 vertices
..	..	..	..	..	..	..	..	..	and 4 faces of tetrahedra
$N_p + N_T + 2$	p_{1,N_T}	p_{2,N_T}	p_{3,N_T}	p_{4,N_T}	f_{1,N_T}	f_{2,N_T}	f_{3,N_T}	f_{4,N_T}	
$N_p + N_T + 3$	N_F								number of faces
$N_p + N_T + 4$	t_1	$q_{1,1}$	$q_{2,1}$	$q_{3,1}$	$t_{1,1}$	$t_{2,1}$			type of face, indices of
..	..	..	..	..	..	..	..	..	the 3 vertices and two
$N_p + N_T + N_F + 3$	t_{N_F}	q_{1,N_F}	q_{2,N_F}	q_{3,N_F}	t_{1,N_F}	t_{2,N_F}			neighboring tetrahedra of face

Table 1: Structure of .msh file

- In line 1 the number N_P of vertices has to be specified.

- Every vertex is given by its Cartesian coordinates. The line number minus 1 is the index of the the vertex.

- After the vertex list the number of tetrahedra N_T is specified.

- Then the list of tetrahedra follows. The line number corresponds to the index of the tetrahedra. Every tetrahedra is characterized by its four vertices. Moreover, the four faces of the tetrahedra are specified by their indices .

- The number of faces N_F of the tetrahedra is specified

- The list of faces follows. Each face is given by its type (first column), its three vertices and the one or two neighboring tetrahedra. The vertex list has to be ordered such that for the first neighboring tetrahedra

$$\det \left| \vec{X}_{q_{2,i}} - \vec{X}_{q_{1,i}}, \vec{X}_{q_{3,i}} - \vec{X}_{q_{1,i}}, \vec{X}_{p_{j,t_{1,i}}} - \vec{X}_{q_{1,i}} \right| \geq 0, \quad j = 1,.,4.$$

holds. Note, the vector $\vec{X}_i$ denotes the vector to a vertex with index i. The indices $q_{1,i}$, $q_{2,i}$, $q_{3,i}$ denote the indices of the three vertices of the face with index i. The index $p_{j,t}$, $j = 1,4$ denote the four vertices of the tetrahedra with index t. $t_{1,j}$ is the first neighboring tetrahedra of the face

with index i. Note, if one of the tetrahedra vertices is on the face, the determinant vanishes. Only for the fourth point it is nonzero. In order to guarantee that the numerical fluxes at the faces have the correct sign, the tetrahedra must be oriented such that this determinant is positive. As a consequence, the determinant for the second tetrahedra is negative.

- The following types of faces exist:

  0: An internal face with two neighboring tetrahedra

  1: A boundary face on the cone, rigid wall. Only one neighboring tetrahedra

  2: An interface to the cylinder at the cylinder head. Numerical fluxes will be calculated by the interface routine.

  3: An interface to the cylinder at the side wall. Depending on the position of the piston, a numerical flux will be determined by the interface routine it will as a solid wall. .

  4: A boundary face at side wall of the valve cylinder, solid wall.

  5: An interface to the valve. Rigid wall when the valve is closed. Mass flow prescribed according to valve model, when valve is open.
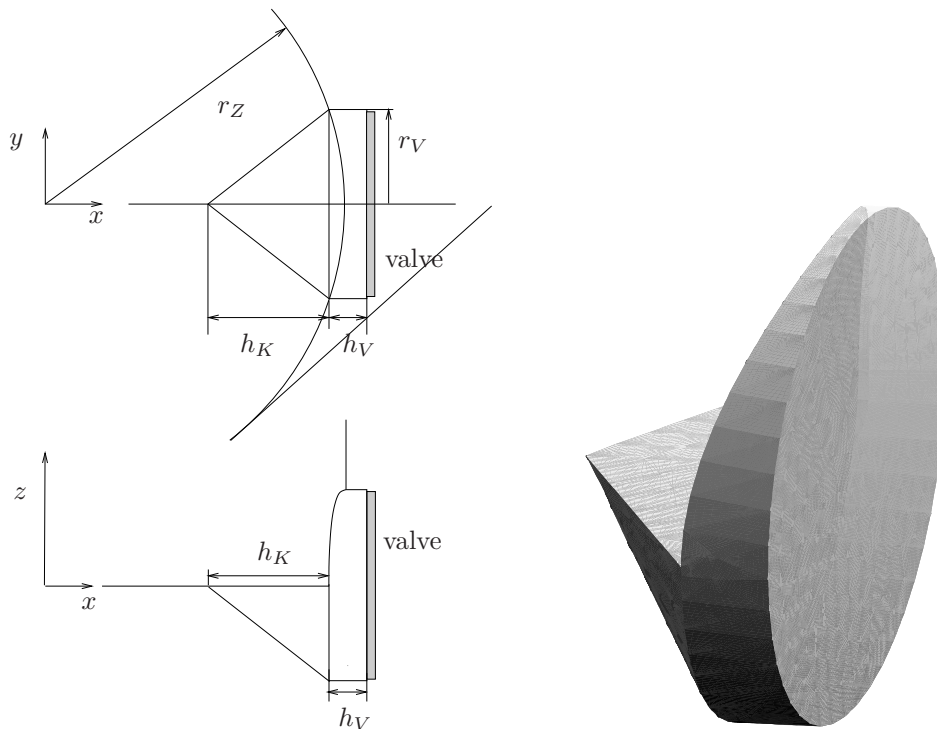
Figure 3: Dimensions of the standard valve pocket: cylinder radius r_Z, valve radius r_V, height of cone h_K, height of valve pocket cylinder h_V

3.2 Numerical method

The numerical method is a first order finite volume method. For each face a numerical is calculated from the cell averages of the two neighboring cells. Characteristics of the method are

- Finite volume scheme on a moving mesh: ALE (Arbitrary Lagrange-Euler formulation).
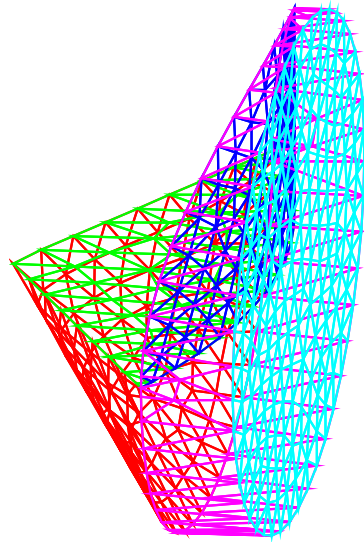
Figure 4: Mesh on surface of valve pocket, Index of surfaces: 1 red, 2 green: interface to cylinder at head , 3 blue: interface at side wall, 4 magenta, 5 light blue: interface to valve

- Time step size according to the CFL (Courant-Friedrichs- Levy) condition.

$$\Delta t = C \frac{1}{|\lambda|_{\max}} \Delta x$$

  where the eigenvalues of the linearized flux function are give by $\lambda = u \pm c$. Here, u is the local flow speed and c the local sound speed. The mesh size Δx is taken to 1/3 of the minimal mesh size in one other coordinate direction. The Courant number C is taken to be 0.7 to account for the skewness of the mesh. For the tetrahedra mesh Δx is chosen as one third of the radius of the inscribed sphere.

- At the interface between the valve pocket and the cylinder, a common partition of the structured and unstructured grid is constructed and the numerical flux for these sub-elements is computed. Special care has to be taken on the side wall, where the structured grid is moving.

- The evaluation of the numerical fluxes is a "grid aligned" Roe-method. For transonic flows a "solution aligned" evaluation of the fluxes is better. This may cause problems in transonic flow regimes.

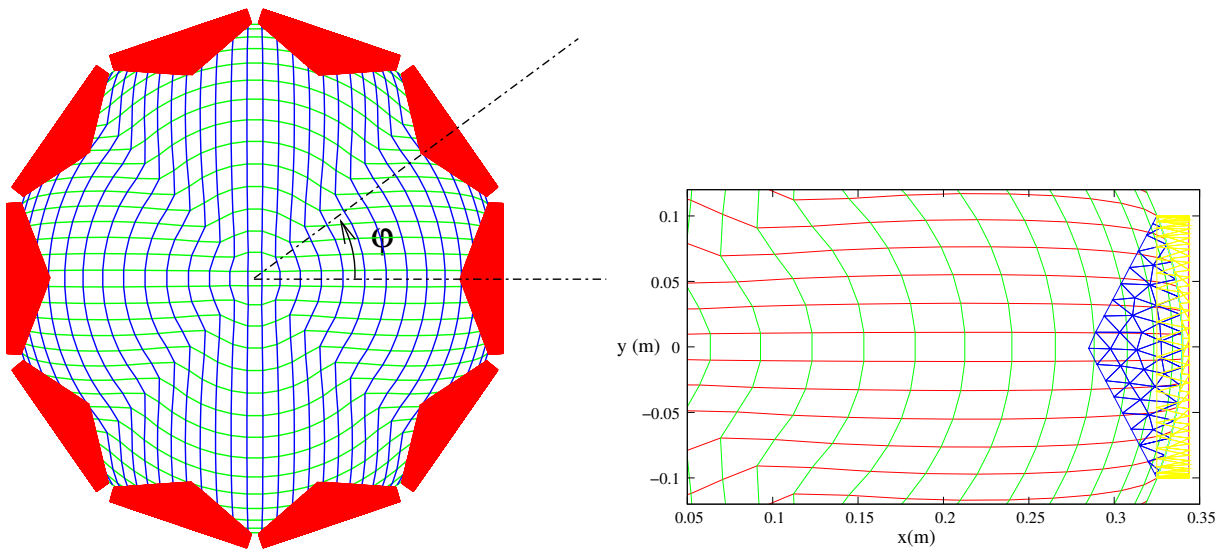Details of the numerical analysis will be described in the forthcoming thesis by Th. Müllner.

Figure 5: Structured grid in cylinder with 15 cells along cylinder radius for compressor with 10 valves (left), interface of structured and unstructured grid at cylinder head (right)
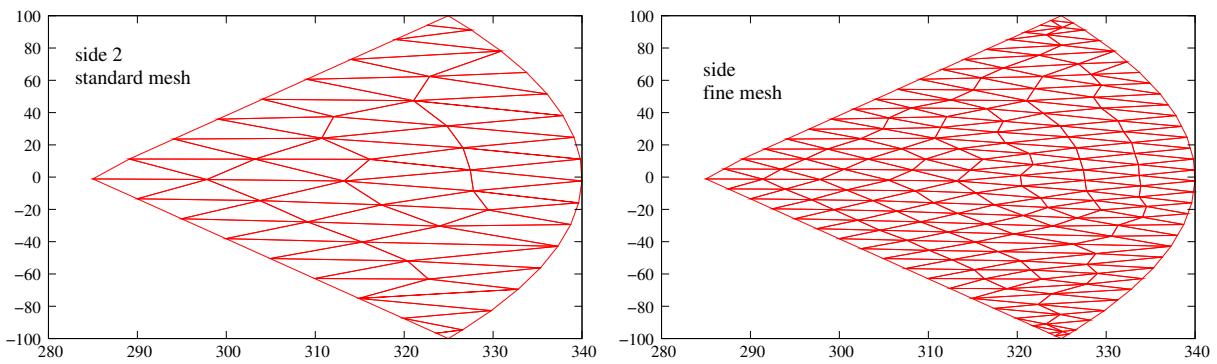

Figure 6: Meshing of the interface to the cylinder head standard mesh (left), refined mesh (right)

4 Program description and handling

4.1 Installation

The setup file for the program can be downloaded from http://www.fluid.tuwien.ac.at/efrc. Executing setup.exe installs the program in a directory which can be chosen. We call it the root directory of the program. The root directory contains a subdirectory called `"ExecutingFiles"`. Here resides `"Compressor3D.exe"` By clicking onto `"Compressor3D.exe"` a GUI (Graphical User Interface) opens. The program can only be used if a valid license is provided. Click on the item "license", then you will get your license status. If no valid license is issued, send the number in the field "licensing information" to the authors of the program. If you are a legitimate user, you will get the necessary license key. The license key is only valid for the specific computer and stored in the file `"license.dat"`.

4.2 Using the Program

Call the program by clicking on Compressor3D.exe in "ExecutingFiles". You can fill out all fields in the GUI or read input files for the cylinder data (see tables 4,5 and the valve data, see tables 6,7,8. These data files can be saved under the item "File" "Save Valve Data", "Save Cylinder Data". figure 7

For the calculation, switch to "Calculation" and enter a case name. A subdirectory of the root directory with the case name will be created if it does not already exist. All information on the current case will be written in this directory: a copy of the cylinder data, valve data, and a file named "Output.txt"containing information for every time step. The meaning of the data in "Output.txt" is listed in the tables 2, 3.

4.3 Changing the unstructured mesh

The reference mesh for the valve pocket is the file `reference_valve_pocket.msh"` in the root directory. If you want to change it, rename your new mesh file to "reference_valve_pocket.msh" and put it in the root directory. A fine mesh for the valve pocket is available on the website.

The name of the mesh file which you enter in the GUI is for internal use only. This file will contain the scaled mesh.

Please note that the program does not check for geometrical conflicts regarding the angular distance between neighboring valves or the deformation of the reference valve pocket.

4.4 Post Processing

The output of the program are the following files:

- `"Casedir/Output.txt` see table 2, 3

- `"Casedir/head/headxxx.txt"`
  `"Casedir/side/sidexxx.txt"`
  `"Casedir/piston/pistonxxx.txt"`
  where xxx is the crank angle.

- If you press "Plot heat transfer" the heat transfer coefficients for every side will be calculated and stored in `"Casedir/alpha_on_HPS.txt"`, and displayed.

- With the button "Plot head/piston/side results" plots of the pressure, density and velocity field on the piston, head and side wall will be generated and stored as .png files in the respective directories.

- For further plots of the data the freely available plot program "gnuplot" can be used. This program resides also in `"ExecutingFiles"`. A description of gnuplot can be found at http://www.gnuplot.info/.
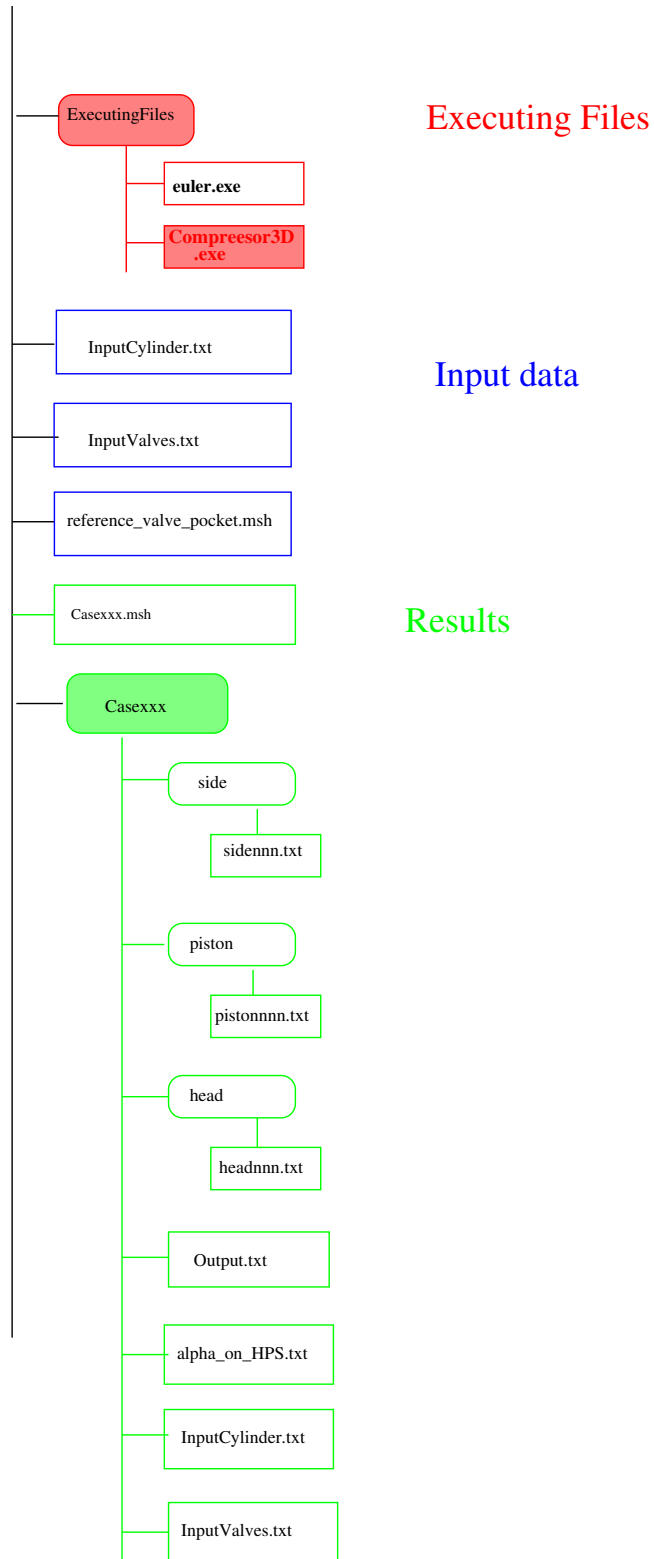
Figure 7: File structure

	quantity	unit
1	number of time step	-
2	time step size	s
3	time	s
4	crank angle φ	-
5	n_3	-
6	$z_{min} + z_P$	m
7	piston velocity v_P	m/s
8	piston force	N
9	piston moment	Nm
10	piston driving power	W
11	Sum Cell Area	
12	Volume	m^3
13	mass	kg
14	density	kg/m^3
15	Total inner energy	J
16	Volume cylinder	m^3
17	mass cylinder	kg
18	Total inner energy cylinder	J
19	mass flow yz-plane	kg/s
20	Volume valve pockets	m^3
21	mass valve pockets	kg
22	total inner energy valve pockets	J

	quantity	unit
23	max. density in cylinder	kg/m^3
24	max. velocity in cylinder	m/s
25	max. pressure in cylinder	Pa
26	maximum eigenvalue in cylinder	m/s
27	max. Mach number in cylinder	1
28	min. density in cylinder	kg/m^3
29	min. pressure in cylinder	Pa
30	max density suction valve pockets	kg/m^3
31	max. velocity suction valve pockets	m/s
32	max pressure suction valve pockets	Pa
33	max. eigenvalue in suction valve pockets	m/s
34	max. Mach number in suction valve pockets	1
35	min. density in suction valve pockets	kg/m^3
36	min. pressure in suction valve pockets	Pa
37	max density in discharge valve pockets	kg/m^3
38	max. velocity in discharge valve pockets	m/s
39	max pressure in discharge valve pockets	Pa
40	max. eigenvalue in discharge valve pockets	m/s
41	max. Mach number in discharge valve pockets	1
42	min. density in discharge valve pockets	kg/m^3
43	min. pressure in discharge valve pockets	Pa

Table 2: Output-data in File Output.txt

column	quantity	unit
$44 + 9(i_v - 1)$	valve lift on valve nr. i_v	m
$45 + 9(i_v - 1)$	valve plate velocity	m/s
$46 + 9(i_v - 1)$	pressure averaged over face 5	Pa
$47 + 9(i_v - 1)$	mass flow face 2	kg/s
$48 + 9(i_v - 1)$	mass flow face 3	kg/s
$49 + 9(i_v - 1)$	mass flow face 5	kg/s
$50 + 9(i_v - 1)$	enthalpy flow face 2	W
$51 + 9(i_v - 1)$	enthalpy flow face 3	W
$52 + 9(i_v - 1)$	enthalpy flow face 5	W

Table 3: Output-data in File Output.txt, Valve numbering: suction valves $i_V = 1,...,n_{SV}$; discharge valves $i_V = n_{SV} + 1,...,n_{SV} + n_{DV}$, n_{SV} number of suction valves, n_{DV} number of discharge valves, order according to list in "InputCylinder.txt" or GUI, resp..

5 Examples

5.1 Two valve compressor

We consider a small compressor with two valves. The data taken here is similar to the test compressor described in Aigner [3]. The basic cylinder and valve data are the same. However, the geometry of the valve pocket is different. The cylinder data is listed in table 4. The numerical parameters are summarized in table 5.

	2-valve comp.	10-valve comp.
Piston diameter d_P (m)	0.22000	0.690
Piston rod diameter d_R (m)	0.00000	0.00
Minimal gap between piston and cylinder-head $z_{\min}$ (m)	0.00150	0.0015
Crank radius r (m)	0.04500	0.075
Con-rod length L (m)	0.30000	0.300
Crank shaft speed omega (rpm)	980.00000	800.00
Ratio of specific heat capacities γ	1.40000	1.4
Suction pressure p_s (Pa)	100000.00000	100000.0
Discharge pressure p_d (Pa)	400000.00000	400000.0
Suction density ρ_s (kg/m^3)	1.00000	1.00

Table 4: Cylinder data

	2-valve comp.	10-valve comp.
Number of cells along piston radius n_1	30 (15)	15
Number of cells along piston rod radius n_2	0	0
Number of cells in clearance n_3	2	2
Radial mesh size grading parameter near piston radius $(0 < \text{grading}_P < 1)$	0.99000	0.9900
Radial mesh size grading parameter near rod radius $(0 < \text{grading}_R < 1)$	0.00000	0.0
Courant number	0.90000	0.9
End computation at crank angle $\varphi_{\max}$ (deg)	420.00000	420

Table 5: Numerical parameters

We compare the simulation results using two different meshes: The standard mesh with 451 vertices and 1203 tetrahedra for a valve pocket and a refined valve pocket mesh with 2548 vertices and 9624 tetrahedra. In the first case, the radius of the inscribed sphere of tetrahedra is between 0.73 mm and 5.9 mm: For the fine mesh, it is between 0.31 mm and 3.0 mm. For the fine mesh, we obtain a step size of

$$\Delta t_{\text{fine}} = \frac{C}{\lambda}\Delta x =\sim \frac{0.9}{300}\frac{1}{3}3\cdot 10^{-4}\sim 3\cdot 10^{-7}\text{s},$$

For the standard mesh, the time step is about $\Delta t_{\text{stand}} \sim 6\cdot 10^{-7}$s. The computation on a single processor laptop was for the standard mesh about 10 h and for the fine mesh about 82 hours, see table 9. One might think, that getting the waves in the cylinder correctly, just increase the number of cells in the cylinder, say $n_R = 30$, but keep the standard mesh for the valve pockets. Unfortunately, in that case a singularity occurred at crank angle 9°. We suppose that the a large discrepancy of the size two neighboring cells might cause a numerical instability. Thus, if a finer resolution is needed, a fine mesh has to be used in the valve pocket, too.

	2-valve comp.	10-valve compr.
Number of suction valves (1)	1	5
z-axis rotation angles for suction valve pockets (°)	108.0	108, 144, 188, 216, 252
Maximum valve plate lift $x_{\mathrm{max_{in}}}$ of suction valve (m)	0.00140	0.0025
Valve parameter $fe_{1\mathrm{mm}}$ of discharge valve (m)	1.86000	5.930
Valve parameter α of discharge valve (1)	2.00000	2.0
Valve parameter β of suction valve ($1/\mathrm{m}^2$)	800000.00000	180000
Valve plate mass of suction valve (kg)	0.07600	0.210
Valve plate force area of suction valve (m^2)	0.00420	0.01781
Valve spring stiffness of suction valve (N/m)	23750.00000	23750.0
Valve spring initial length of suction valve (m)	0.00050	0.000750

Table 6: Data suction valves

	2-valve comp.	10-valve comp.
Number of discharge valves (1)	1	5
z-axis rotation angles for discharge valve pockets (°)	288	288, 324, 360, 36, 72
Maximum valve plate lift $x_{\mathrm{max_{out}}}$ of discharge valve (m)	0.00140	0.0025
Valve parameter $fe1\mathrm{mm}$ of discharge valve (m)	1.86000	5.930
Valve parameter α of discharge valve (1)	2.00000	2.00
Valve parameter β of discharge valve ($1/\mathrm{m}^2$)	800000.00000	800000.
Valve plate mass of discharge valve (kg)	0.07600	0.210
Valve plate force area of discharge valve (m^2)	0.04200	0.01781
Valve spring stiffness of discharge valve (N/m)	50000.00000	23750.0
Valve spring initial length of discharge valve (m)	0.00110	0.000750

Table 7: Data discharge valves

	2-valve comp.	10-valve comp.
Valve radius r_{v1} (mm)	60.00000	100.0
Height of valve cone h_{k1} (mm)	12.00000	40
Height of valve pocket h_{v1} (mm)	22.00000	19.0

Table 8: Dimensions of the valve pockets

cells along radius	mesh in valve pocket	comp. time $CA = 420°$
15	standard	10 h 23 min
30	standard	sing. at $CA = 9°$
30	fine	81 h 48 min

Table 9: Computation time for standard and fine mesh for 2-valve compressor

In figure 8 the pressure at the discharge and suction valve is shown over the crank angle. The results for both meshes agree reasonably well. Only during discharge a difference in the pressure at the suction valve can be noticed. For the fine mesh, this pressure is smaller. We interpret this result that the expansion wave which reduces the pressure at the suction side during discharge is less damped in case of a finer grid compared to the standard grid.

This observation is confirmed by considering the pressure difference across the compressor, see figure 9. Here again, the difference is small. Moreover, the internal wave, which can be observed after the closing of the discharge valve, is damped less in the case of the finer grid compared to the standard grid.

In figure 10 the difference between the maximum pressure and the minimum pressure in the suction valve pocket, the discharge valve pocket, and the cylinder is shown for both grids. The largest differences occur in the discharge valve pocket at the beginning of discharge. At the end of discharge, the pressure differences in the cylinder dominate. Again a difference of about 20% percent can be observed between the results of the fine and the standard mesh calculation.

The behavior of the discharge valve is identical for both meshes, see figures 11 and 12.

In figure 13 the mass flow through the faces of the valve pockets are shown. The normal vector is directed out of the valve pocket. Thus, a positive mass flow is directed out of the valve pocket. During expansion ($0° <$Crank angle $< 50°$) gas is flowing out of both valve pockets into the cylinder. During intake ($50° <$ crank angle $< 180°$) gas enters through face 5 (valve and leaves the suction valve pocket through face 2, which is the interface to the cylinder head. The mass flow through the interface to the side wall is negligible. During compression, gas is pressed equally into both valve pockets. During discharge the gas enters the valve pocket through face 2 and leaves through 5. The mass flow through face 3 is again very small.

The heat transfer coefficient for head, piston, and sidewall are shown in figure 17. During expansion and discharge, they are almost grid-independent. However, during intake, they differ markedly. As a possible reason, we suspect that the numerical dissipation in case of the standard grid damps the internal flow velocity and thus, reduces the heat transfer coefficients. The vertical flow velocities at the side wall are shown as contour plots during intake and discharge in figure 14 and figure 16, respectively. It can be observed that during intake, the flow field differs qualitatively for both meshes. The "black spots" in figure 14 for the fine mesh indicate a negative, downward velocity near the suction valve. Thus, we expect a jet from the suction valve into the cylinder which sucks in gas from the surroundings. For the standard mesh, the flow situation is qualitatively different, with an upward velocity near the suction valve.

During outflow, the velocity fields for bot both meshes are almost identical. This behavior is reflected in the (dis-)agreement of the heat transfer coefficients for both the flow situations at CA=100° and CA=300°, respectively.
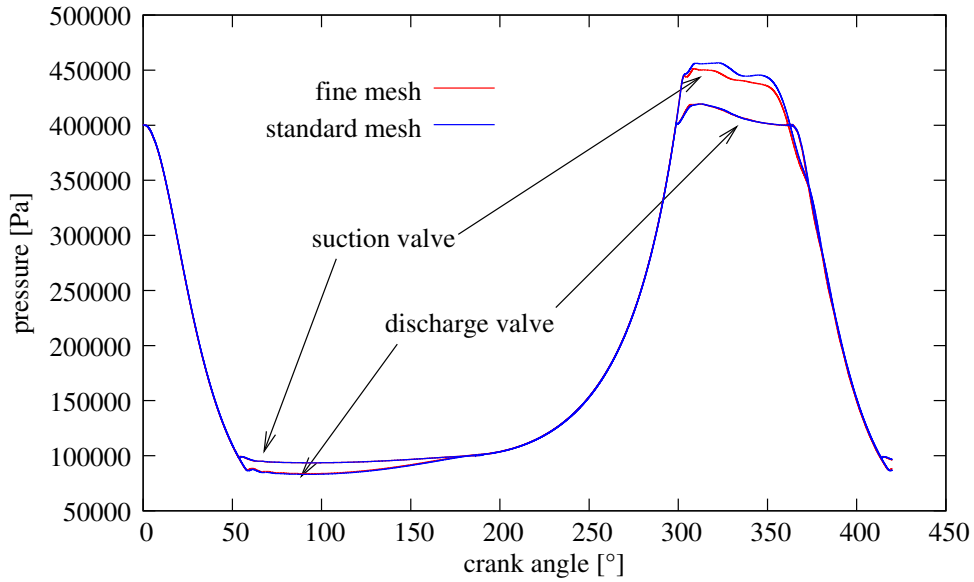
Figure 8: Pressure in suction and discharge valve pocket. Numerical results for fine and standard mesh
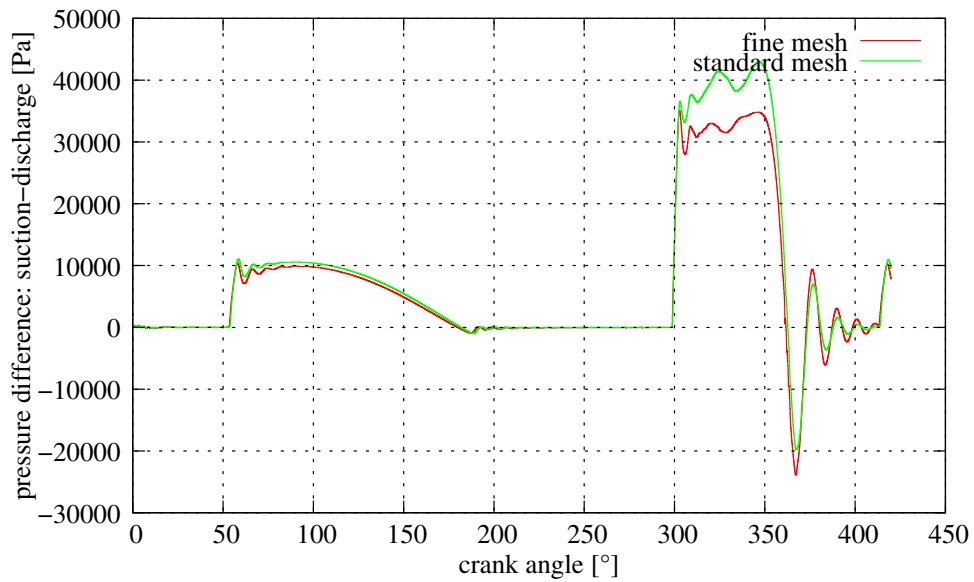

Figure 9: Pressure difference between suction and discharge valve pocket. Numerical results for fine and standard mesh
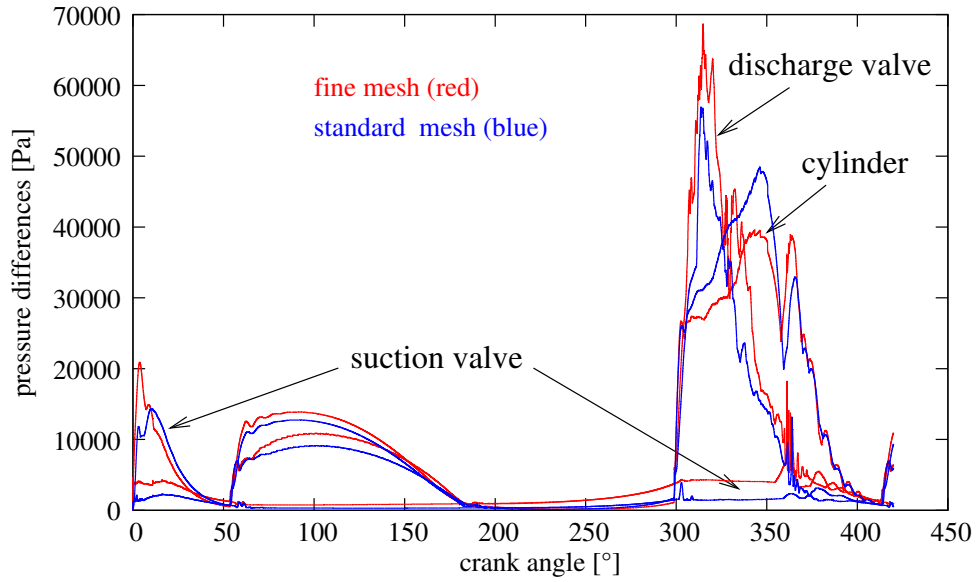
Figure 10: Difference between maximum and minimum pressure in the cylinder, the suction, and the discharge valve pocket, res. Numerical results for the fine and the standard mesh
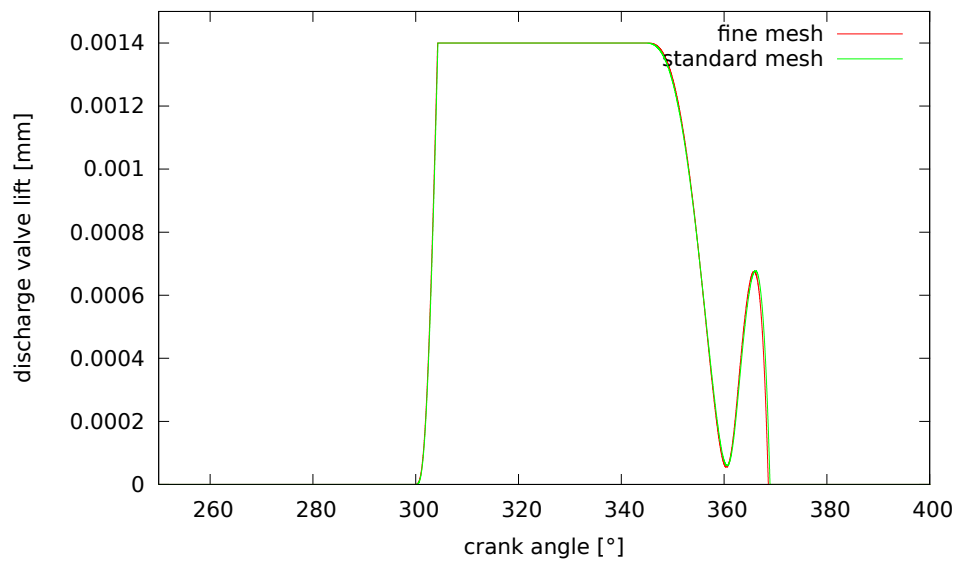

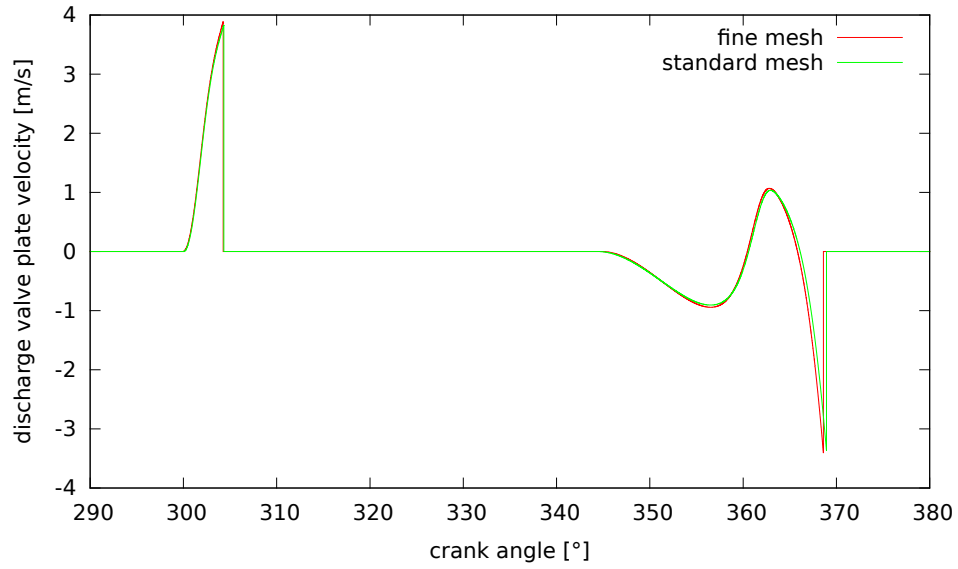Figure 11: Valve plate lift of discharge valve. Numerical results for fine and standard mesh

Figure 12: Valve plate velocity of discharge valve. Numerical results for fine and standard mesh
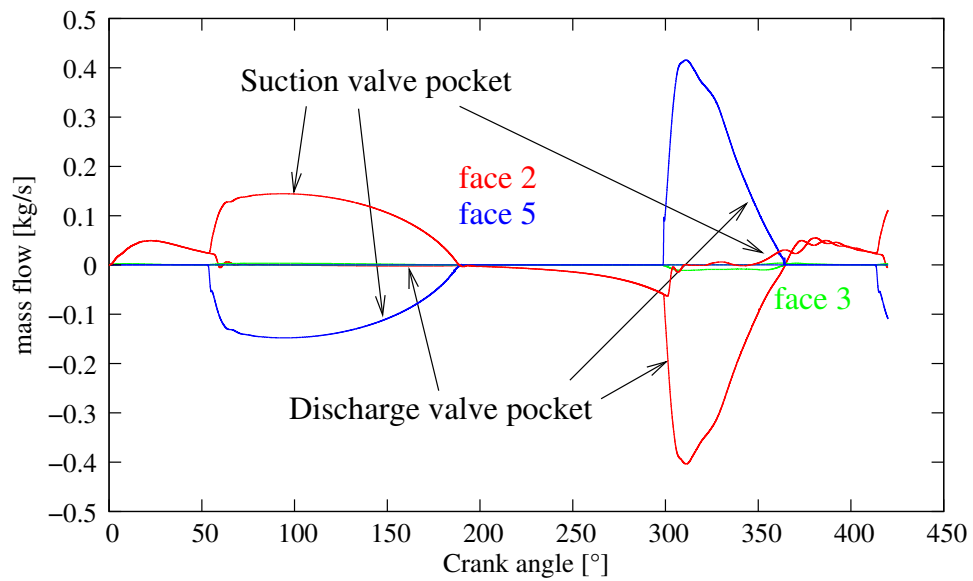
Figure 13: Mass flow through faces 2,3, and 5 of the valve pockets. The normal vector is directed outward of the valve pocket
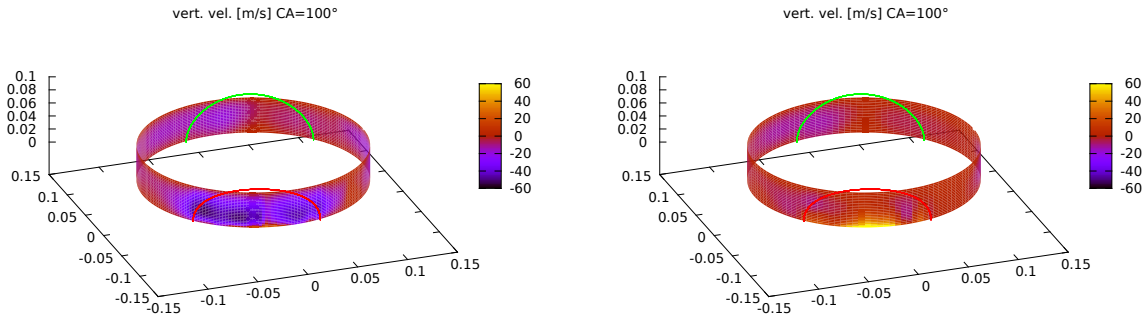
Figure 14: Vertical velocity at side wall for CA=100°: fine mesh (left), standard mesh (right)
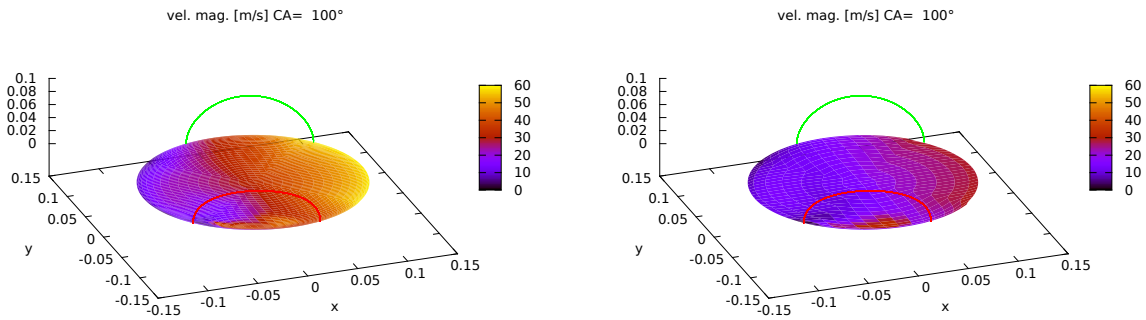
Figure 15: Velocity magnitude at cylinder head for CA=100°: fine mesh (left), standard mesh (right)
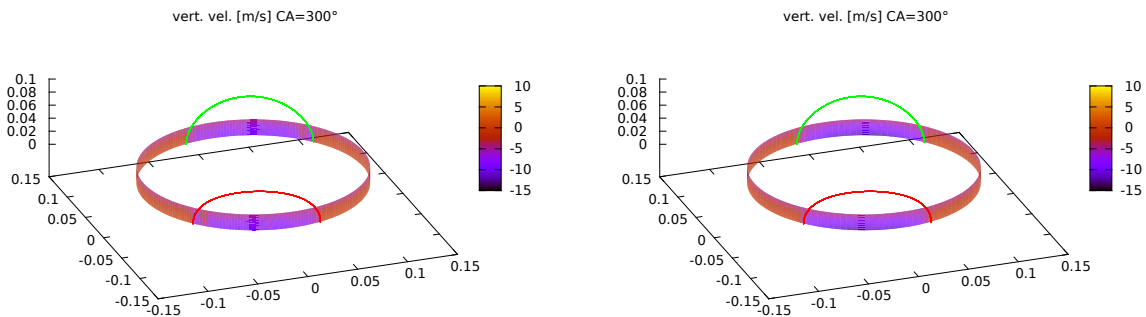

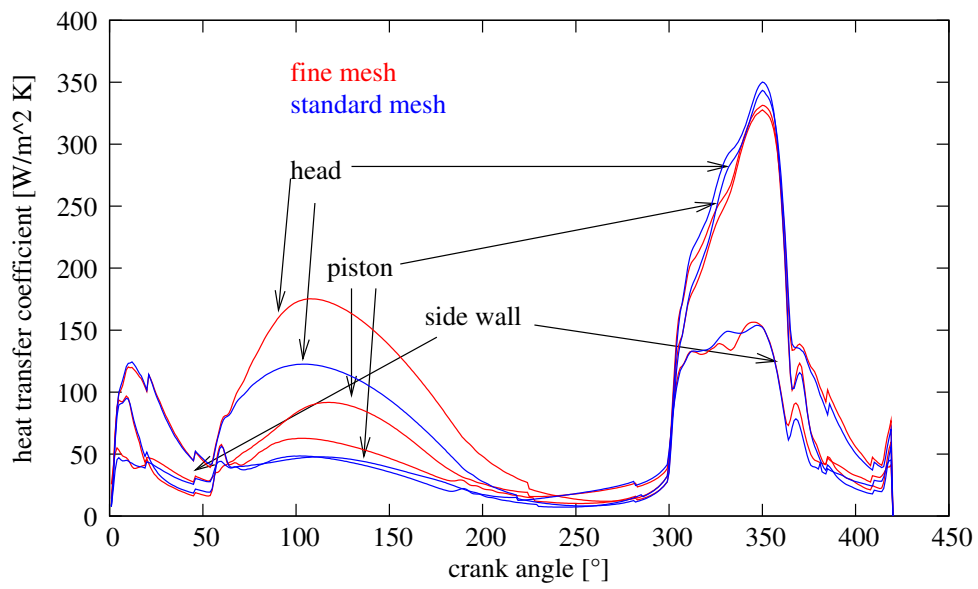Figure 16: Vertical velocity at side wall for CA=300°: fine mesh (left), standard mesh (right)

Figure 17: Heat transfer coefficient. Numerical results for fine and standard mesh

5.2   10-valve compressor

As second example, we present the simulation of a ten-valve compressor. The data of the simulation is listed in tables 4-8. The corresponding input files are part of the release of Compressor3D.

In figure figtenvpressure the pressures in the central discharge and suction valves are shown. An internal wave during discharge can be observed from the fact the pressure at the suction valve drops significantly and recovers again.

In figure 19, the closing behavior of the discharge valves is shown. While the central valve closes almost perfectly, the lateral and mid valves bounce back several times.

In figure 20 the velocity field along the piston during intake is shown. Figures 21,22 show contour plots of the pressure along the piston and the temperature along the side wall.
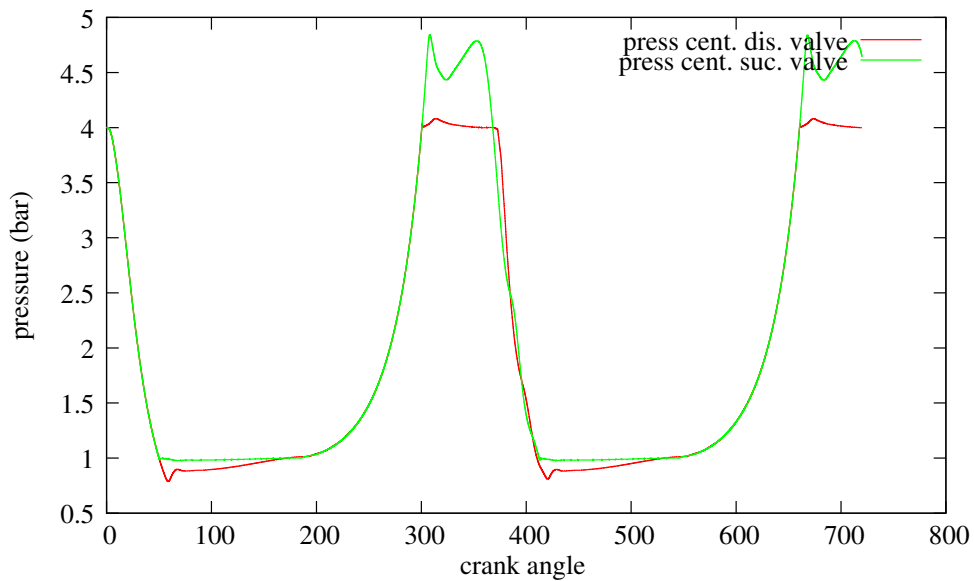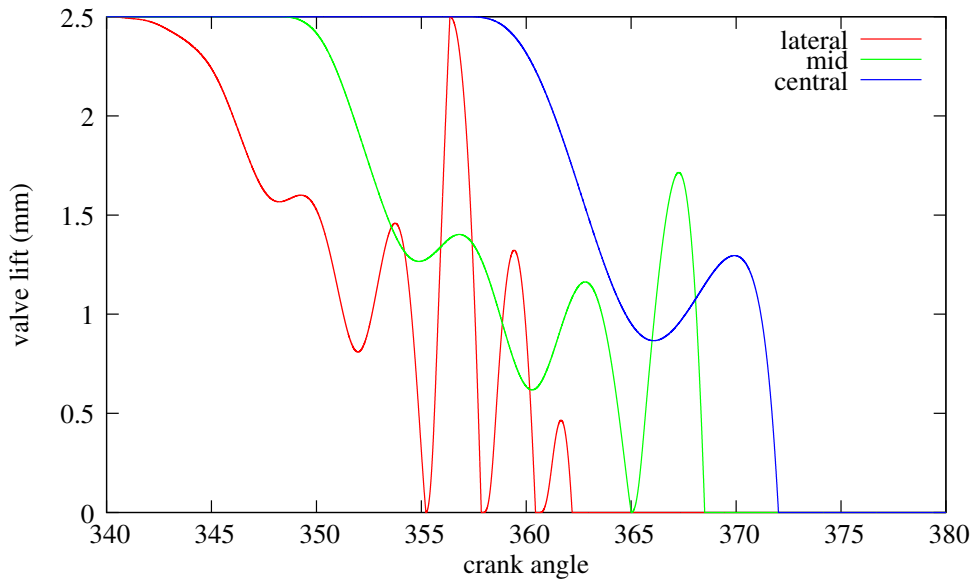

Figure 18: Pressure
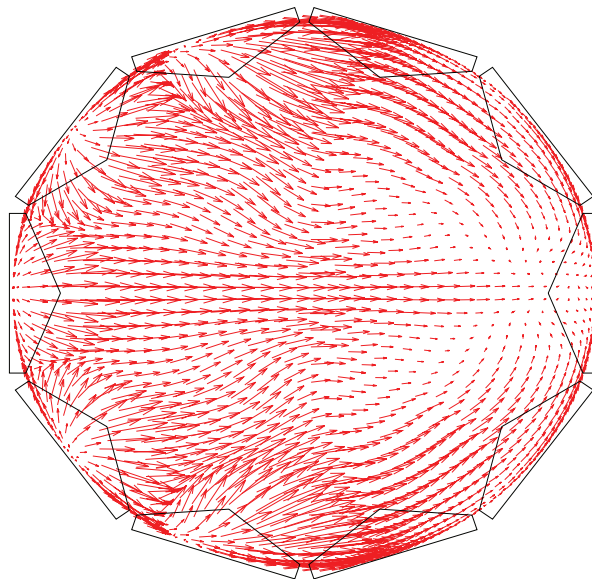
Figure 19: Valve lift discharge valves

Figure 20: Velocity at Piston CA=420°

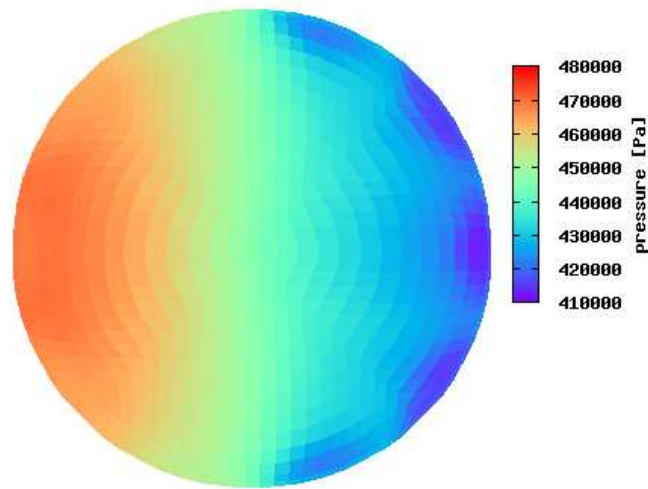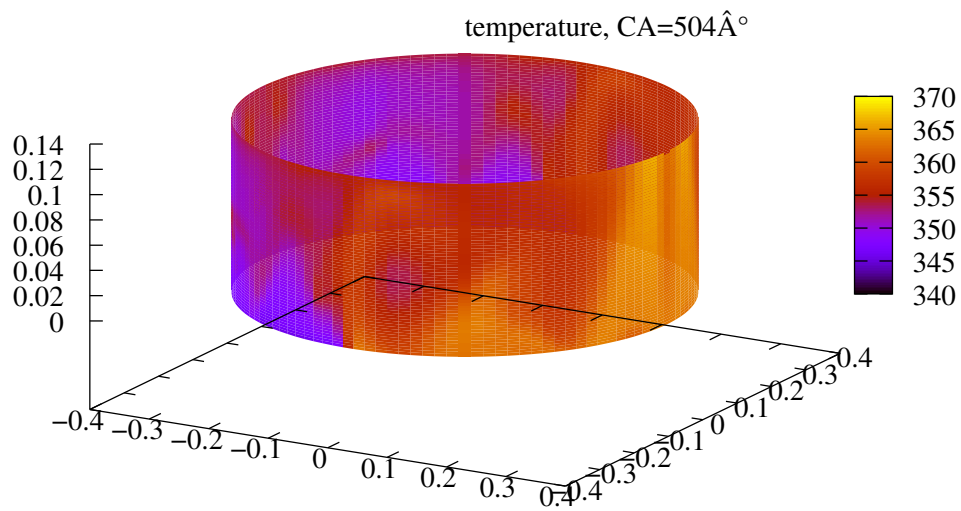Figure 21: Pressure at piston CA=306°

Figure 22: Temperature at side wall CA=504°

6 Conclusions

A 3D-Euler flow simulation program for reciprocating compressors has been developed. Inside the cylinder, a structured moving mesh uses automatic re-meshing when the aspect ratio of the cells is beyond certain limits. An unstructured tetrahedral mesh is used in the valve pockets. A novel strategy coupling the flow domains inside the cylinder and the valve pockets by a common partition of both meshes at the interfaces has been developed. The program works stable as long as certain safety measures are obeyed (ratio of cell sizes at interfaces), and the flow field is in some sense reasonable (subsonic flow).

However, there are still options to improve the program handling.

- At the moment, the caloric material for air is hard coded. Materials data for other gases will be provided in the next release.

- New reference valve pocket mesh files.

- Full boundary-layer calculation for improving the heat transfer coefficients.

References

[1] R. Aigner. *Internal Flow and Valve Dynamics in a Reciprocating Compressor* . Ph-D thesis, Technische Universität Wien, 2007.

[2] R. Aigner, G. Meyer, and H. Steinrück. Valve dynamics and internal waves in a reciprocating compressors. In 4th *EFRC Conference*, pages 169–178, 2005.

[3] R. Aigner and H. Steinrück. Modelling fluid dynamics, heat transfer and valve dynamics and in a reciprocating compressors. In 5th *EFRC Conference*, pages 169–178, 2007.

[4] K. Schlichting, H. Gersten. *Boundary-layer theory.* Springer, 8th edition, 2000.

[5] J. Zierep. *Grundzüge der Strömungslehre.* Springer, 1997.